



1        **Long-term trend of ozone pollution in China during 2014-**  
2                    **2020: distinct seasonal and spatial characteristics**

3        Wenjie Wang<sup>1</sup>, David D. Parrish<sup>2</sup>, Siwen Wang<sup>1</sup>, Fengxia Bao<sup>1</sup>, Ruijing Ni<sup>3</sup>, Xin Li<sup>4</sup>,  
4        Suding Yang<sup>4</sup>, Hongli Wang<sup>5</sup>, Yafang Cheng<sup>3</sup>, Hang Su<sup>1\*</sup>

5

6

7        <sup>1</sup> Multiphase Chemistry Department, Max Planck Institute for Chemistry, Mainz, 55128,  
8        Germany.

9        <sup>2</sup> David. D. Parrish, LLC, Boulder, CO, 80303, USA.

10       <sup>3</sup> Minerva Research Group, Max Planck Institute for Chemistry, Mainz 55128, Germany.

11       <sup>4</sup> State Key Joint Laboratory of Environmental Simulation and Pollution Control,  
12       College of Environmental Sciences and Engineering, Peking University, Beijing,  
13       100871, China.

14       <sup>5</sup> State Environmental Protection Key Laboratory of Formation and Prevention of  
15       Urban Air Pollution Complex, Shanghai Academy of Environmental Sciences,  
16       Shanghai 200233, China.

17

18

19

20

21

22

23

24       \* Corresponding author.

25

26                Address: Multiphase Chemistry Department, Max Planck Institute for Chemistry,

27        Mainz 55128, Germany.

28                Email: h.su@mpic.de

29

30

31

32

33

34

35

36

37

38



39 **Abstract:** In the past decade, ozone ( $O_3$ ) pollution has become a severe environmental  
40 problem in major cities in China. Here, based on available observational records, we  
41 investigated the long-term trend of ozone pollution in China during 2014–2020. Ozone  
42 concentrations were higher in urban areas than in non-urban areas. During these seven  
43 years, the highest ozone concentrations primarily occurred in summer in northern China,  
44 and in autumn or spring in southern China. Although ozone precursors, including  
45 nitrogen oxides ( $NO_x$ ) and carbon monoxide (CO), continuously decreased throughout  
46 the seven years, four ozone metrics that were used to characterize ozone exposure levels  
47 increased from 2014 to 2017 and reached a plateau after 2017. The long-term trend of  
48 ozone concentrations differed across seasons; especially from 2019 to 2020 when ozone  
49 concentrations decreased in summer and increased in winter. To analyze the causes of  
50 this observed trend, a photochemical box model was used to investigate the change in  
51 ozone sensitivity regime in two representative cities – Beijing and Shanghai. Our model  
52 simulations suggest that the summertime ozone sensitivity regime in urban areas of  
53 China has changed from a VOC-limited regime to a transition regime during 2014–  
54 2020; by 2020, the urban photochemistry is in a transition regime in summer but in a  
55 VOC-limited regime in winter. This study helps to understand the distinct trends of  
56 ozone in China and provides insights into efficient future ozone control strategies in  
57 different regions and seasons.

58  
59  
60



## 61 **1 Introduction**

62 Tropospheric ozone (O<sub>3</sub>) is an air pollutant that is detrimental to human health,  
63 vegetation and ecosystem productivity (Ainsworth et al., 2012; Mills et al., 2018; Monks  
64 et al., 2015; Fiore et al., 2009). The inhalation of ozone impairs the functioning of the  
65 human respiratory and cardiovascular systems through its reaction with the lining of  
66 the lung and other surfaces in the respiratory tract (Jindal, 2007). Ozone is also an  
67 important greenhouse gas that leads to positive radiative forcing (Stocker et al., 2014).  
68 A comprehensive characterization of the spatial (latitude, longitude and altitude) and  
69 temporal distribution of tropospheric ozone is critical to our understanding of these  
70 issues. Here we summarize this distribution over China from the available observational  
71 records to the extent possible.

72 China has undergone rapid economic development, leading to higher demand for  
73 energy, and greater usage of fossil fuels during the past several decades. As a result,  
74 high anthropogenic emissions to the atmosphere have produced severe ozone pollution  
75 in urban areas of China, where daily maximum 8-hour average (MDA8) ozone  
76 concentrations often exceed the standard of 80 ppb (Li et al., 2014; Li et al.,  
77 2019a; Zhang et al., 2014; Lu et al., 2018). In contrast to the generally decreasing ozone  
78 levels in the United States and Europe, available surface ozone observations have  
79 widely shown significant upward trends in China since 1990 in rural areas (Xu et al.,  
80 2008; Wang et al., 2009; Ma et al., 2016; Sun et al., 2016; Xu et al., 2016; Xu et al., 2018),  
81 urban areas (Li et al., 2019a; Wang et al., 2020; Zhang et al., 2014; Lu et al., 2018), and  
82 over regional scales (Verstraeten et al., 2015; Xu and Lin, 2011). China has become a  
83 global hot spot of ground-level ozone pollution. The present annual mortality attributed  
84 to long-term ozone exposure in China is estimated to be ~50,000 to 316,000 deaths (Liu  
85 et al., 2018; Malley et al., 2017).

86 Global model simulations suggest that the average lifetime of ozone in the  
87 troposphere is about 22 days (Stevenson et al., 2006; Young et al., 2013). In the free  
88 troposphere at northern midlatitudes, where prevailing westerly winds dominate, the



89 net ozone lifetime is considerably longer, and is greater than the transport time around  
90 the Earth (Trickl et al., 2011). Consequently, the increase in ozone in China not only  
91 influenced domestic public health, but also influenced downwind countries (Brown-  
92 Steiner and Hess, 2011; Lin et al., 2012) and thus increased global background ozone  
93 concentrations. Several studies indicate that rising Asian emissions influenced baseline  
94 ozone concentrations in America and Europe through the hemispheric transmission of  
95 ozone and its precursors (Cooper et al., 2010; Verstraeten et al., 2015). The baseline  
96 ozone concentrations at northern midlatitudes increased at an average rate of  $\sim 0.60$  ppb  
97 year<sup>-1</sup> from 1980 to 2000 (Parrish et al., 2020). Such an increase in baseline ozone  
98 concentrations makes it more difficult to further reduce ozone in America and Europe.  
99 Therefore, a detailed characterization of ozone pollution in China will aid  
100 understanding of the variation in baseline ozone and guide the reduction of ozone  
101 throughout northern midlatitudes.

102 Despite several studies of the ozone trends in specific rural or urban sites in China  
103 (Ma et al., 2016; Gao et al., 2017; Zhang et al., 2014; Lu et al., 2018), detailed  
104 characterization of spatial distribution and temporal trend of ozone in different seasons  
105 across China remains scarce. In addition, it is not yet well understood how changes in  
106 precursor emissions influence the trend of ozone in China. Chinese government  
107 launched the Air Pollution Prevention and Control Action Plan in 2013–2017 and the  
108 Clean Air Action plan in 2018–2020 to reduce anthropogenic emissions (Cheng et al.,  
109 2019). Since 2013, the surface monitoring network has been greatly expanded, and  
110 detailed hourly data across China became available from China Ministry of Ecology  
111 and Environment (<https://quotsoft.net/air/>). The goal of this study is to elucidate the  
112 spatial distribution, seasonal variation and temporal trends of ozone in China by using  
113 these surface ozone observations to characterize multiple ozone metrics relevant to  
114 human health. Quantifying the detailed spatial distribution and temporal trend of ozone  
115 across China will provide a better understanding of the response of ozone to emission  
116 reductions, and inform the development of control measures to effectively mitigate  
117 ozone in the future.



## 118 2 Method

### 119 2.1 Measurements

120 Hourly surface O<sub>3</sub>, nitrogen dioxide (NO<sub>2</sub>) and carbon monoxide (CO)  
121 concentrations during 2014–2020 were obtained from the public website of the China  
122 Ministry of Ecology and Environment (MEE) (<https://quotsoft.net/air/>). The surface  
123 monitoring network covered 940 stations in summer 2014, and extended to 1669  
124 stations by 2020 (~330 cities). The O<sub>3</sub> concentrations at 750 sites with continuous  
125 observations over these 7 years were analyzed. These measurements document the air  
126 quality in Chinese cities and have been analyzed in recent studies (Li et al., 2019a; Lu  
127 et al., 2018). Total solar radiation data in 2013 were acquired from the meteorological  
128 data set of fundamental meteorological elements of China national weather station  
129 (V3.0), but data after 2013 are unavailable.

130 Urban and non-urban sites are distinguished by population density. Population  
131 density data were acquired from Gridded Population of the World (GPW), v4;  
132 <https://sedac.ciesin.columbia.edu/data/set/gpw-v4-population-density-rev11>. This is a  
133 dataset of the world population gridded at ~5 km resolution. According to the China  
134 Statistical Yearbook in 2018 (China Statistics Press, 2018), China's urban population  
135 density was 2500 people/km<sup>2</sup>. In the following analysis, urban sites correspond to  
136 population density  $\geq 2500$  people/km<sup>2</sup>, and non-urban sites correspond to population  
137 density  $< 2500$  people/km<sup>2</sup>.

138 To reflect the breadth of different health-related indicators used globally, four  
139 metrics—AVGMDA8, 4MDA8, NDGT70, 3MMDA1—are used here to characterize  
140 ozone pollution levels. The definitions of these metrics are given in **Table 1**.  
141 AVGMDA8 represents the mean value of daily maximum 8 h average (MDA8) ozone  
142 concentrations, and 4MDA8 represents the annual 4th highest (MDA8) ozone  
143 concentrations; 3MMDA1 represents the annual maximum of the 3-month running  
144 mean of the daily maximum 1-hour (MDA1) ozone concentrations. Since these metrics  
145 are determined from different parts of the distribution of ozone concentrations, their



146 spatial distribution and temporal variation may differ. We derived all metrics from the  
147 hourly measurements that were filtered by data quality control procedures following  
148 the Tropospheric Ozone Assessment Report (TOAR) data completeness requirements  
149 and procedures. The calculations of AVGMDA8, 4MDA8, NDGT70 are based on  
150 MDA8 ozone concentrations. MDA8 ozone concentration is the maximum value of 8-  
151 hour running averages calculated from 0 h to 23 h local time. Note that if the data  
152 availability at a certain site is less than 60% (i.e., less than 5 hours for 8-hour averages  
153 or 15 hours for one day), the MDA8 value was considered missing. For the calculation  
154 of these metrics (AVGMDA8, 4MDA8, NDGT70), if less than 60% of MDA8 values  
155 are available (i.e., less than 220 MDA8 values for a year or 55 MDA8 values for a  
156 season), the annual mean or seasonal mean values of the metrics at a certain site were  
157 considered missing. The calculation of 3MMDA1 was based on the daily maximum 1-  
158 hour (MDA1) ozone value. Similar to the MDA8 ozone value, if less than 60% of data  
159 are available (i.e. less than 15 hours for one day), the MDA1 value at a certain site was  
160 considered missing. For the calculation of 3MMDA1, if less than 60% of MDA1 values  
161 are available (i.e. less than 55 MDA1 values for three months and 220 MDA1 values  
162 for a year), the 3MMDA1 value at a certain site was considered missing.

163 Beijing and Shanghai are the two largest cities in China and have undergone severe  
164 ozone pollution in the past decade (Wang et al., 2020; Xu et al., 2019). Measurement  
165 data in Beijing and Shanghai were analyzed to show the variation characteristic of  
166 ozone sensitivity regimes. The data of O<sub>3</sub>, NO<sub>2</sub> and CO were acquired from the public  
167 website of the China Ministry of Ecology and Environment (<https://quotsoft.net/air/>).  
168 Volatile organic compounds (VOCs), and meteorological factors (including  
169 temperature, relative humidity, photolysis frequencies and air pressure) were measured  
170 during 2014–2020 at two representative urban sites in Beijing and Shanghai: Peking  
171 University and Shanghai Academy of Environmental Sciences. Temporal trends and  
172 composition of VOCs at the two sites were considered to be representative across  
173 Beijing and Shanghai (Wang et al., 2010; Xu et al., 2011; Zhang et al., 2012). VOCs  
174 were measured using a commercial GC-FID/PID system (Syntech Spectra GC955  
175 series 600/800 analyzer).



## 176 2.2 Zero-dimension photochemical box model

177 A zero-dimension photochemical box model was used to simulate the sensitivity  
178 of ozone production and loss to its precursor concentrations. Compared with regional  
179 3-D models, the box model has the advantage that it can be constrained by  
180 comprehensive measurements to eliminate the uncertainty from emission inventories.  
181 The box model includes MCM v.3.3.1 as the chemical mechanism. Hourly averages of  
182 CO, NO<sub>2</sub>, NO, O<sub>3</sub>, SO<sub>2</sub>, VOCs (56 species), formaldehyde, acetaldehyde, photolysis  
183 frequencies, temperature, air pressure, and relative humidity were used as model  
184 constraints. HONO was not measured, and thus was calculated according to the  
185 concentration of NO<sub>2</sub> and the observed ratio of HONO to NO<sub>2</sub> in Beijing (Hendrick et  
186 al., 2014). The model simulations were performed in a time-dependent mode with spin-  
187 up of two days. For physical removal processes, a 24-h lifetime was assumed for all  
188 simulated species, which approximately simulates the effects of dilution and surface  
189 deposition. This modeling approach has been used previously (Wang et al., 2019; Wang  
190 et al., 2020).

191 RO<sub>2</sub>, HO<sub>2</sub> and OH radicals were simulated by the box model to calculate the net  
192 ozone production rate (P(O<sub>3</sub>)) and ozone loss rate (L(O<sub>3</sub>)) as shown in Equation (1) and  
193 (2) as derived by Mihelcic et al. (2003).

$$194 \quad P(O_3) = k_{HO_2+NO}[HO_2][NO] + \sum_i(k_{RO_2+NO}^i[RO_2^i][NO]) - k_{OH+NO_2}[OH][NO_2] -$$
$$195 \quad L(O_3) \quad (1)$$

$$196 \quad L(O_3) = (\theta j(O^1D) + k_{OH+O_3}[OH] + k_{HO_2+O_3}[HO_2] +$$
$$197 \quad \sum_j(k_{alkene+O_3}^j[alkene^j])[O_3] \quad (2)$$

198 where  $\theta$  is the fraction of O<sup>1</sup>D from ozone photolysis that reacts with water vapour, and  
199  $i$  and  $j$  represent the number of species of RO<sub>2</sub> and alkenes, respectively.



## 200 **3 Results and Discussion**

### 201 **3.1 The spatial distribution and seasonal variation of ozone pollution**

202 **Figure 1** presents the spatial distributions of the mean values of four ozone metrics  
203 (AVGMDA8, 4MDA8, NDGT70 and 3MMDA1) at non-urban and urban sites in China  
204 during 2014–2020. The spatial distribution was similar between urban and non-urban  
205 sites for all four metrics; for example, warm-season AVGMDA8 O<sub>3</sub> concentrations at  
206 74% of urban sites and 67% of non-urban sites exceed the air quality standard Grade 1  
207 limit of 50 ppb. Hot spots of ozone pollution mainly occurred in the more economically  
208 developed areas in northern, eastern and central China. At both urban and non-urban  
209 sites, the highest regional average ozone concentrations occur in the North China Plain  
210 with the average warm-season AVGMDA8 O<sub>3</sub> concentration of 66 ppb, significantly  
211 higher than the corresponding national average value of 54 ppb. Although the solar  
212 radiation in the North China Plain is not the strongest across China (Jiang et al., 2019),  
213 North China Plain has a large density of urban and industrial activities. Previous studies  
214 denote that the North China Plain has the highest NO<sub>x</sub> and VOCs emissions over China  
215 (Liu et al., 2016; Li et al., 2019b). This clearly indicates that ozone pollution is closely  
216 related to anthropogenic activities.

217 The month in which the 3MMDA1 ozone concentration occurred is defined as the  
218 middle month in the 3 months of 3MMDA1, which can indicate the season when  
219 maximum ozone pollution occurred. As shown in **Fig. 2**, the month in which the  
220 3MMDA1 ozone concentration occurred shows a significant spatial variation. In most  
221 years, the 3MMDA1 ozone concentration in northern China (north of the Yangtze River)  
222 occurred mainly in summer (June, July and August), whereas in southern China (south  
223 of the Yangtze River), it occurred in autumn (September, October and November) or  
224 spring (March, April, May). In northern China, sunlight intensity is highest in summer  
225 and photochemical production from anthropogenic and biogenic precursors maximizes.  
226 In southern China, the southwest monsoon prevails in summer leading to an inflow of  
227 marine air with low ozone concentrations and reduced photochemical ozone production



228 due to more cloudy and rainy weather (Yin et al., 2019); thus in this region the highest  
229 ozone usually appears in autumn when sunlight intensity maximizes.

230 It is notable that the 3MMDA1 ozone concentration mainly occurred in spring in  
231 both Heilongjiang and Yunnan provinces, which are located in northeast and southwest  
232 China, respectively. This is consistent with a previous study reporting that Yunnan  
233 province and northeast China had peak O<sub>3</sub> in spring 2014–2017 (Yin et al., 2019). A  
234 springtime maximum was also found for the column O<sub>3</sub> in Yunnan retrieved from  
235 satellite data (Xiao and Jiang, 2013). The occurrence of maximum ozone concentrations  
236 in spring has been attributed to several factors, including 1) the peak occurrence of  
237 stratospheric intrusions, 2) photochemistry of precursors built up during winter, and 3)  
238 biomass-burning either as forest fires or for land clearance (Monks et al., 2015).  
239 Heilongjiang province is located in the northernmost part of China (43°26'N–53°33'N)  
240 with relatively low temperature and light intensity, and thus its photochemical  
241 production of ozone is weak all year round. We surmise that the springtime maxima of  
242 ozone in this province is due to the first two causes: the stratospheric intrusion of ozone  
243 in spring (Stohl et al., 2003), and ozone production in spring from accumulated  
244 precursors that were emitted from coal burning for heating during the wintertime.  
245 Yunnan province is located in a plateau area with average altitude of 2000 m; the  
246 elevated terrain of this province is more likely to be influenced by the descending free  
247 tropospheric air masses with high ozone concentrations from the stratospheric origin  
248 (Stohl et al., 2003; Cooper et al., 2012). Additionally, higher sunlight intensity in spring  
249 at this lower latitude province is also conducive to photochemical production of ozone.

250 We also compared the seasonal variations in MDA1 ozone concentrations in three  
251 typical Chinese city clusters, Beijing-Tianjin-Hebei (BTH), Yangtze River Delta (YRD)  
252 and Pearl River Delta (PRD) (**Fig.3**). In each city cluster there is a distinct seasonal  
253 ozone pattern: a sharp unimodal distribution with a summer maximum in BTH, a broad  
254 distribution with a spring maximum in YRD, and a less distinct, unimodal distribution  
255 with an autumn maximum in PRD. Meteorological factors determine the different  
256 ozone distribution patterns; most importantly PRD and YRD received more  
257 precipitation in summer than BTH, and that PRD was especially affected by the inflow



258 of marine air during the southwest monsoon. Furthermore, in PRD typhoons led to less  
259 cloud cover, and thus more solar radiation in autumn, which accelerated O<sub>3</sub> production  
260 (Qu et al., 2021). As shown in **Fig. 3**, the seasonal variations in ozone in the three city  
261 clusters are overall consistent with those of solar radiation in representative cities of the  
262 three city clusters (Beijing in BTH, Shanghai in YRD and Guangzhou in PRD). This  
263 result indicates that the local photochemistry driven by solar radiation plays a crucial  
264 role in ozone seasonal variations.  
265

### 266 **3.2 Temporal trend of ozone pollution**

267 Ozone trends measured on regional scales, in urban areas, and at rural sites in  
268 previous studies are summarized in **Table 2**. For direct comparison of these results  
269 reported in different units, we have included estimated trends in units of % yr<sup>-1</sup> for all  
270 studies. Xu and Lin (2011) and Verstraeten et al. (2015) have reported that tropospheric  
271 ozone concentrations increased in summer during 1979–2005 in the North China Plain  
272 and 2005–2010 in Eastern China at a rate of 1.1% and 3.0% yr<sup>-1</sup>, respectively, based on  
273 satellite measurements. Urban ozone concentrations increased significantly in Beijing,  
274 Shanghai, Hongkong, Sichuan Basin and other cities during the past one to two decades  
275 at rates of 2.0 to 6.7% yr<sup>-1</sup> (Gao et al., 2017; Cheng et al., 2016; Wang et al., 2020; Chen  
276 et al., 2021; Li et al., 2020; Lu et al., 2018). A significant increase in ozone (+1.6% yr<sup>-1</sup>)  
277 was detected at Shangdianzi, a rural site in the North China Plain (Ma et al., 2016). A  
278 moderate increase was detected at the global background site (Waliguan site) in western  
279 China (+0.44% yr<sup>-1</sup>) (Xu et al., 2018; Xu et al., 2020). No significant trend was detected  
280 at either the eastern coastal Changdao site (Wang et al., 2020) or the Longfengshan site  
281 on the northeastern edge of China (Xu et al., 2020). The only significant decrease was  
282 reported at the Akedala site on the northwestern edge of China (-3.3% yr<sup>-1</sup>) (Xu et al.,  
283 2020). In general, these studies show that ozone concentrations in China have risen in  
284 the past three to four decades.

285 **Figure 4** summarizes variations of four ozone metrics (warm season AVGMDA8,  
286 4MDA8, 3MMDA1 and NDGT70) during 2014–2020 for Chinese urban and non-urban



287 sites. **Figure A1** presents the spatial distribution of warm season AVGMDA8 ozone  
288 concentrations at urban and non-urban sites for each year during 2014–2020. These four  
289 metrics at urban sites were overall higher than at non-urban sites by 3.5%, 6.6%, 4.2%  
290 and 16%, respectively (**Fig. 4**). These results in China differ from those in Europe and  
291 North America, where the mean levels of these metrics at non-urban sites are similar to  
292 those at urban sites (Fleming et al., 2018), although there are differences in the  
293 approaches to classifying sites as urban or non-urban. The possible reason for the  
294 difference is that transported background ozone dominates over local and regional  
295 photochemical production in Europe and North America, while local photochemistry  
296 dominates ozone levels in China. From 2014 to 2020, the trends of ozone were generally  
297 similar between urban and non-urban sites. The four metrics all increased from 2014 to  
298 2017, but remained relatively stable after 2017 despite being significantly higher in  
299 2019. The elevated ozone level in 2019 was related to higher temperatures in the warm  
300 season (Li et al., 2020). Overall, the rapid increase in ozone concentrations in China  
301 has either slowed or ended (depending upon metric) after 2017. In **Fig. 4**, the variations  
302 in the four metrics are fitted by quadratic functions. The quadratic polynomial  
303 coefficients are all negative and statistically significant for the four metrics, which is  
304 strong evidence that the increasing trend has slowed.

305 Because the trends of ozone are generally similar between urban and non-urban  
306 sites (**Fig. 4**), the nationwide (including both urban and non-urban) AVGMDA8 was  
307 used to analyze ozone trends for different seasons. **Figure 5** shows variations in  
308 seasonal and annual AVGMDA8 during 2014–2020. For the national average,  
309 AVGMDA8 was highest in summer, followed by spring, autumn, and winter. This  
310 metric increased in all four seasons from 2014 to 2017, with the fastest increase in  
311 spring ( $3.1 \text{ ppb yr}^{-1}$ ,  $r^2=0.94$ ), followed by winter ( $2.9 \text{ ppb yr}^{-1}$ ,  $r^2=0.91$ ), summer ( $2.0$   
312  $\text{ppb yr}^{-1}$ ,  $r^2=0.90$ ) and autumn ( $1.2 \text{ ppb yr}^{-1}$ ,  $r^2=0.81$ ). The annual average increased at  
313 a rate of  $2.0 \text{ ppb yr}^{-1}$  ( $r^2=0.95$ ) from 2014 to 2017. The more rapid increase of ozone  
314 concentration in spring than in summer resulted in a decrease in the gap between the  
315 two seasons. This is consistent with a recent study reporting that ozone pollution in the  
316 North China Plain extended to the spring season (Li et al., 2021). After 2017,



317 AVGMDA8 remained relatively stable in summer and spring, but still increased  
318 significantly in autumn and winter. Compared with 2019, the seasonal average MDA8  
319 ozone concentration decreased by 5.5 ppb in summer 2020, but increased by 5.1 ppb in  
320 winter 2020. **Figure 6** illustrates the spatial patterns of the summer and winter changes  
321 in seasonal average MDA8 O<sub>3</sub> from 2019 to 2020. In summer ozone decreased  
322 significantly in most regions of China, with greater decreases in central China and the  
323 North China Plain. In winter, ozone increased significantly throughout China. The  
324 cause of these changes will be discussed in Section 3.3.

325 The trends of the ozone precursors, NO<sub>2</sub> and CO, were investigated based on the  
326 observational data. As shown in **Fig. 7**, both NO<sub>2</sub> and CO decreased significantly from  
327 2014 to 2020 for both annual and seasonal averages. Notably, NO<sub>2</sub> decreased faster  
328 after 2017 than before 2017. Both the MEIC inventory and OMI NO<sub>2</sub> data show a  
329 decrease during 2013-2019 (Shah et al., 2020), which is consistent with our result. The  
330 emission inventory suggests that VOC emissions were stable during 2013-2019 in  
331 China (Li et al., 2019b;Zheng et al., 2021). In 2020 VOCs, CO and NO<sub>x</sub> emissions  
332 decreased significantly in winter but only slightly in summer, compared to 2019 (Zheng  
333 et al., 2021), which is consistent with the changes of measured NO<sub>2</sub> and CO (**Fig. 7**).

### 334 **3.3 The impact of photochemistry on ozone temporal trend**

335 Ozone concentrations are influenced by photochemical processes that depend on  
336 precursor concentrations and meteorological conditions. Changes in ozone precursor  
337 emissions, particularly VOC and NO<sub>x</sub>, are the primary factors driving ozone trends in  
338 China. The relationship between O<sub>3</sub> and its precursor concentrations is generally  
339 nonlinear—a decrease in precursor concentrations does not necessarily result in a  
340 corresponding decrease in O<sub>3</sub> concentration. Differing responses of ozone production  
341 to VOC and NO<sub>x</sub> emission changes allow three ozone sensitivity regimes to be  
342 distinguished: VOC-limited, NO<sub>x</sub>-limited and transition regimes (Kleinman,  
343 1994;Kleinman et al., 1997). In this section, based on comprehensive measurements in  
344 Beijing, the impact of photochemical regimes on the temporal trend of ozone in urban



345 areas of China was discussed.

346 As discussed in Section 3.2, in summer when ozone pollution is most severe,  
347 ozone increased from 2014 to 2017, but remained relatively stable after 2017 (**Fig. 5**).  
348 To explore the impact of photochemical regimes on the temporal trend of ozone in  
349 summer, the zero-dimensional photochemical box model constrained by long-term  
350 measurements in Beijing and Shanghai was used to examine the variation in the  
351 sensitivity of ozone to precursor emissions. In this study, we focused on the effects of  
352 photochemistry on ozone sensitivity to precursors; transport effects were not considered.  
353 The ozone sensitivity regime was diagnosed by testing the response of  $P(O_3)$  as  
354 calculated from Equation (1) to the changes of VOCs and  $NO_x$  concentrations (**Fig. 8**).  
355 The box model simulations suggest that in Beijing VOC reduction would significantly  
356 decrease ozone during all seven years, while  $NO_x$  reduction would significantly  
357 increase ozone during 2014–2017 but only slightly increase ozone in 2018 and slightly  
358 decrease ozone during 2019–2020. The 2014–2018 results are consistent with the VOC-  
359 limited regime in which a reduction in VOCs is effective in mitigating ozone production,  
360 while a reduction in  $NO_x$  increases ozone production. The 2019–2020 results are  
361 consistent with the transition regime in which reductions of either VOCs or  $NO_x$  can  
362 decrease ozone production. These results indicated that the summertime photochemical  
363 environment in Beijing shifted from a VOC-limited regime to a transition regime. The  
364 Shanghai simulations show similar behavior in terms of the shift in the photochemical  
365 regime.

366 Previous 3-D model studies have reported results similar to our box model  
367 simulation; urban areas in China were in the VOC-limited regime in the summer of  
368 2013–2017, but in the transition regime after 2017 (Shao et al., 2021; Kang et al.,  
369 2021; Li et al., 2019a). Tang et al. (2021) showed that ozone production in Beijing was  
370 transitioning from VOC-sensitive to  $NO_x$ -sensitive over the 2013–2018 period. The  
371 sharp decrease in  $NO_x$  combined with a smaller change in VOCs in Shanghai has led  
372 to a shift in the  $O_3$  production from a VOC-limited regime to a  $NO_x$ -limited regime  
373 over the past decade (Xu et al., 2019). In addition to model studies, satellite-observed  
374  $HCHO/NO_2$  ratios also indicate that there is a shift in the North China Plain, YRD and



375 PRD from the VOC-limited regime to the transitional regime, which is associated with  
376 a rapid drop in anthropogenic NO<sub>x</sub> emissions from 2016 to 2019 (Wang et al., 2021).  
377 These studies agree that ozone sensitivity in summer in urban areas of China has  
378 gradually changed from a VOC-limited regime to a transition or NO<sub>x</sub>-limited regime  
379 due to faster decreases in NO<sub>x</sub> emissions than in VOC emissions over the past decade.  
380 Therefore, we surmise that the rapid increase of summertime ozone during 2013-2017  
381 is due to the decrease in NO<sub>x</sub> under VOC-limited conditions, and that the slowing of  
382 the summertime ozone increase after 2017 is due to decreased NO<sub>x</sub> emissions and  
383 relatively stable VOC emissions under the transition regime conditions. This finding  
384 lends more confidence to the effective reduction in summertime ozone through  
385 continued reductions in VOC and NO<sub>x</sub> emissions.

386 Another issue is that compared to 2019, MDA8 ozone concentrations decreased in  
387 summer but increased in winter in 2020 (**Fig. 5 and 6**) despite the decrease of both NO<sub>x</sub>  
388 and CO concentrations (**Fig. 7**). Based on measurements in Beijing in 2019, the  
389 observation-based box model was used to examine the sensitivity of ozone to precursors  
390 in summer and winter. As shown in **Fig. 9**, in the summer of 2019, Beijing was in the  
391 transition regime, when reductions in VOCs and NO<sub>x</sub> both decreased the integrated  
392 ozone production rate. In winter it was in the VOC-limited regime, when reduction in  
393 VOCs decreased, but reduction in NO<sub>x</sub> increased, the ozone production rate. This result  
394 demonstrates that summer and winter had different ozone sensitivity characteristics in  
395 2019. Based on WRF-Chem model simulations, Kang et al. (2021) also reported that  
396 ozone sensitivity entered the transition or NO<sub>x</sub>-limited regime in summer 2020, but was  
397 still in the VOC-limited regime in winter 2020. In addition, the WRF-Chem model  
398 results by Le et al. (2020) indicate that the chemical regime was VOC-limited during  
399 the COVID-19 pandemic lockdown in winter 2020 in China and the decrease in NO<sub>x</sub>  
400 led to significant ozone increases. These studies are consistent with our simulation  
401 results in Beijing. The difference in ozone sensitivity regimes between winter and  
402 summer is likely to be a crucial cause of opposite ozone changes between winter and  
403 summer in 2020. Although ozone production rates and concentrations are much smaller  
404 in winter, ozone can influence particulate matter (PM) formation through increasing the



405 atmospheric oxidizing capacity in this season (Le et al., 2020). Therefore, different  
406 ozone sensitivity regimes between winter and summer should be fully considered to  
407 effectively mitigate both ozone and PM in the two seasons.

#### 408 **4 Conclusions**

409 During the past decade, China has devoted substantial resources to improving the  
410 environment. These efforts reduced atmospheric particulate matter loading, but ambient  
411 ozone levels increased (Shao et al., 2021). We present a detailed characterization of the  
412 spatial distribution and temporal trend of ozone over China based on nationwide hourly  
413 ozone observations, and find that:

414 (1) Maximum ozone concentrations primarily occur in summer in northern China, but  
415 in autumn or spring in southern China. Meteorological factors, especially solar  
416 radiation and the southwestern monsoon, play key roles in the regional contrast of the  
417 seasonal variations.

418 (2) Four ozone metrics (AVGMDA8, 4MDA8, NDGT70, 3MMDA1) increased from  
419 2014 to 2017, and remained relatively stable after 2017. These metrics were generally  
420 higher at urban sites than at non-urban sites. The trend of ozone concentrations differed  
421 across seasons; especially from 2019 to 2020 when ozone concentrations decreased in  
422 summer and increased in winter.

423 (3) Simulations by an observationally constrained box model and previous 3-D model  
424 simulations agree that the ozone sensitivity in summer in urban areas of China gradually  
425 changed from the VOC-limited regime to a transition regime. This increases our  
426 confidence in the reduction of both VOC and NO<sub>x</sub> emissions as an effective approach  
427 to further reducing summertime ozone. Box model simulations also indicate that the  
428 urban photochemistry is still in the VOC-limited regime in winter in 2020.

429 Our study provides an improved understanding of the past and future response of  
430 ozone to emission reductions in China, and can inform control measures for effective  
431 future reductions of ozone.

432



433

#### 434 **Data availability**

435 The observational data and model code used in this study are available from  
436 corresponding authors upon request (h.su@mpic.de).

#### 437 **Author contributions**

438 HS and WW designed the research. WW and HS prepared the manuscript with  
439 contributions from other authors. WW performed data analysis with contributions from  
440 DP, SW, RN, FB and YC. HW, XL, SY collected data.

#### 441 **Competing interests**

442 The authors declare that they have no known competing financial interests or personal  
443 relationships that could have appeared to influence the work reported in this paper.

#### 444 **Acknowledgements**

445 This study is support by the Max Planck Society (MPG). Y.C. thanks the Minerva  
446 Program of MPG.

447

448

449

450

451

452

453

454

455

456

457

458

459

460

461

462

463

464

465

466

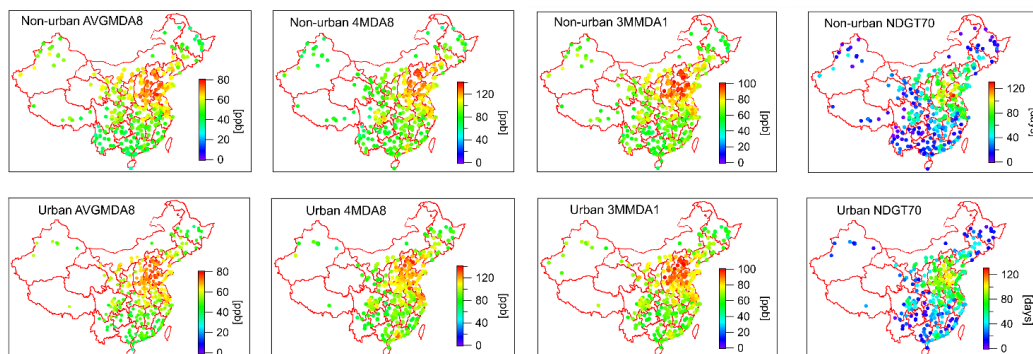
467

468



469

470



471

472 Figure 1. Spatial distribution of four ozone metrics (AVGMDA8, 4MDA8, 3MMDA1,  
473 NDGT70) at urban and non-urban sites averaged over 2014–2020. AVGMDA8 is the  
474 mean MDA8 O<sub>3</sub> in the warm season (April to September); other metrics are annual  
475 values.

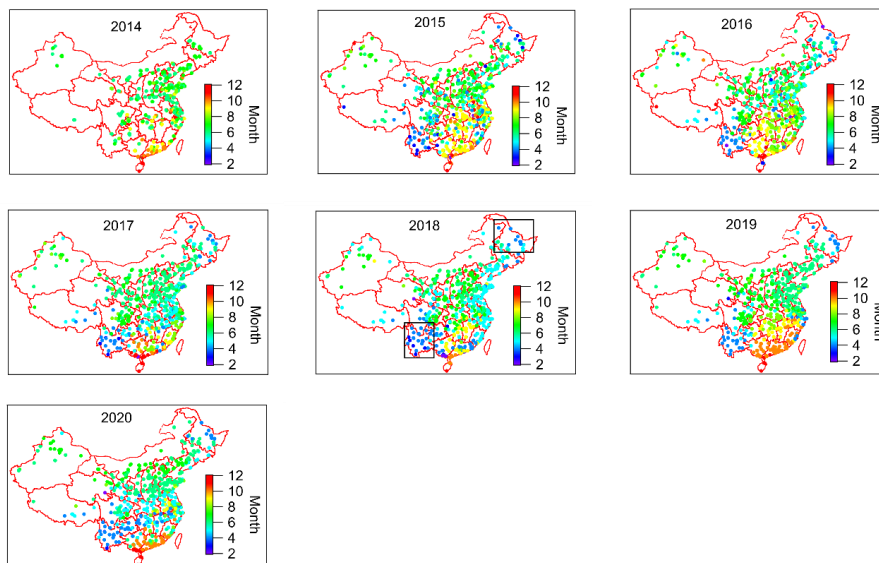
476

477



478

479



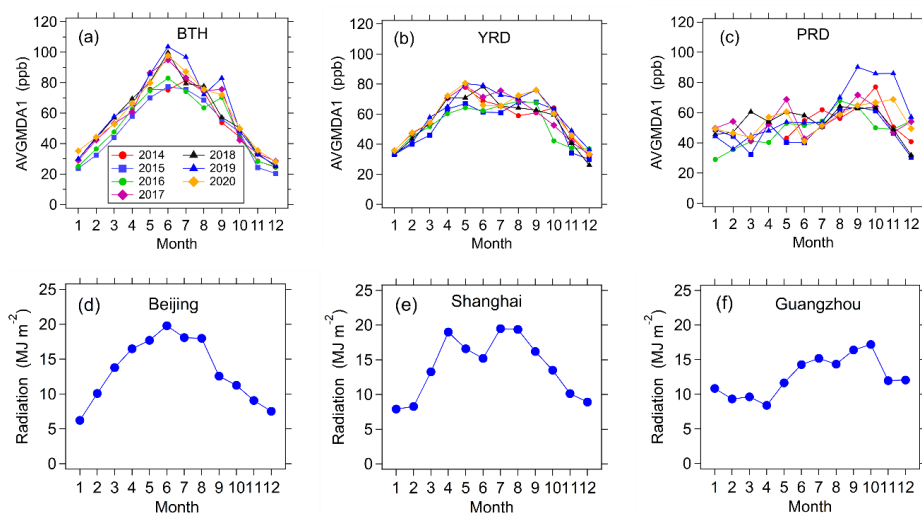
480 Figure 2. Spatial distribution of the month in which 3MMDA1 ozone concentration  
481 occurred during 2014-2020. Rectangles included in the 2018 map in the northeast and  
482 southwest China represents the Heilongjiang and Yunnan provinces, respectively.

483



484

485



486

487 Figure 3. (a), (b) (c): Seasonal variations in monthly mean MDA1 ozone concentrations  
488 over all sites in BTH, YRD and PRD during 2014-2020. (d), (e), (f): Seasonal variations  
489 in monthly mean solar radiation in representative cities of the three city clusters (Beijing  
490 in BTH, Shanghai in YRD and Guangzhou in PRD) in 2013.

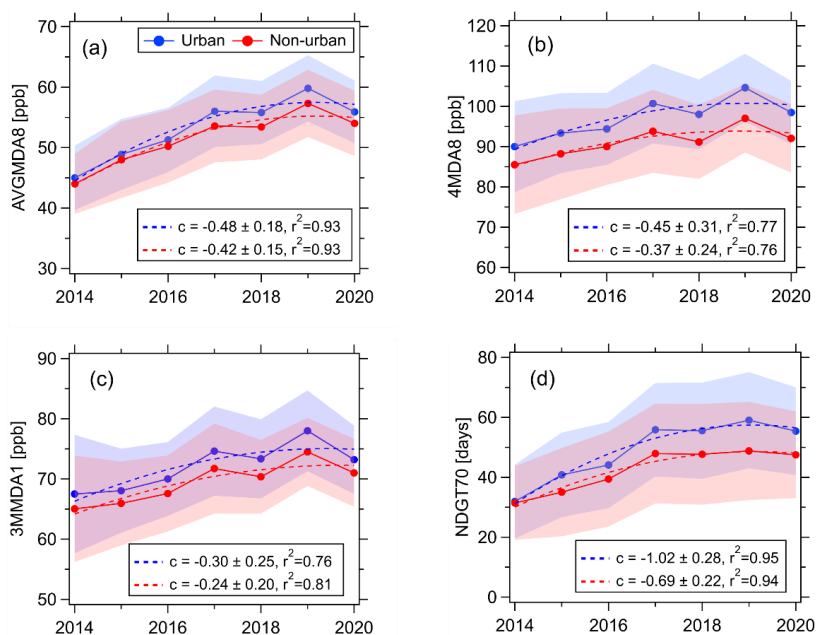
491



492

493

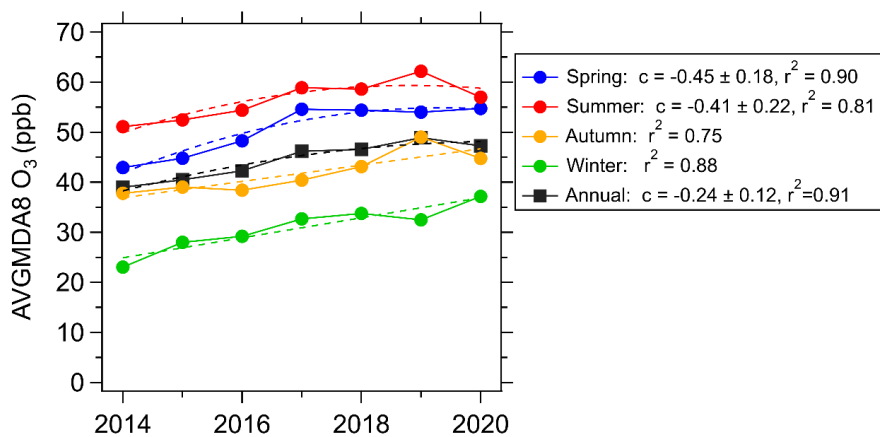
494



495 Figure 4. Variations in four ozone metrics (AVGMDA8, 4MDA8, 3MMDA1 and  
496 NDGT70) at urban and non-urban sites during 2014-2020. AVGMDA8 is the mean  
497 MDA8 O<sub>3</sub> in the warm season (April to September), and the other metrics are annual  
498 values. Shaded areas represent the range of mean values  $\pm$  the 50% standard deviation  
499 for each metric. The dashed lines are fitted by the polynomial function ( $y=a+bx+cx^2$ ).  
500 The quadratic polynomial coefficient  $c$  ( $\pm$  one standard deviation) and the determination  
501 coefficient  $r^2$  are given.  
502



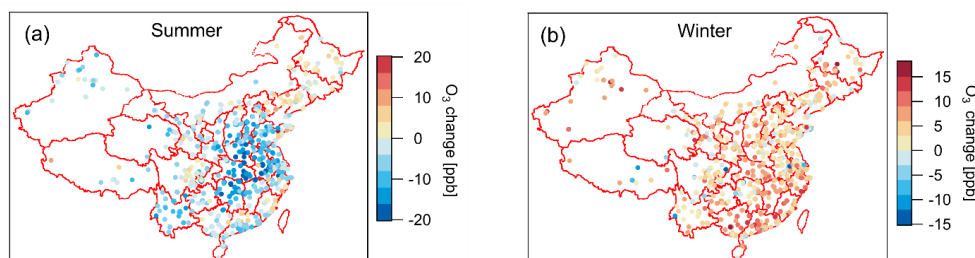
503  
504  
505



506 Figure 5. Variations in seasonal and annual AVGMDA8 O<sub>3</sub> levels during 2014–2020.  
507 The trends for spring, summer and annual averages are fitted by the polynomial  
508 function ( $y=a+bx+cx^2$ ) and the trends for autumn and winter are fitted by the linear  
509 function ( $y=a+bx$ ). The quadratic polynomial coefficient  $c$  ( $\pm$  one standard deviation)  
510 and the determination coefficient  $r^2$  are given.  
511



512  
513  
514  
515

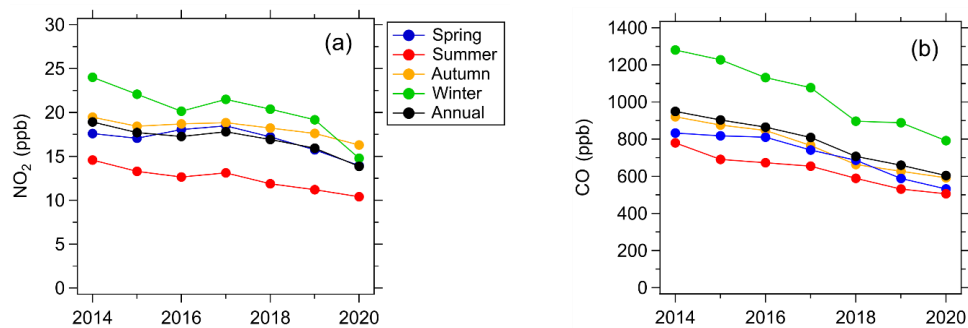


516 Figure 6. The change in seasonal averages of MDA8 O<sub>3</sub> from 2019 to 2020 in summer  
517 (a) and winter (b), China.  
518



519

520

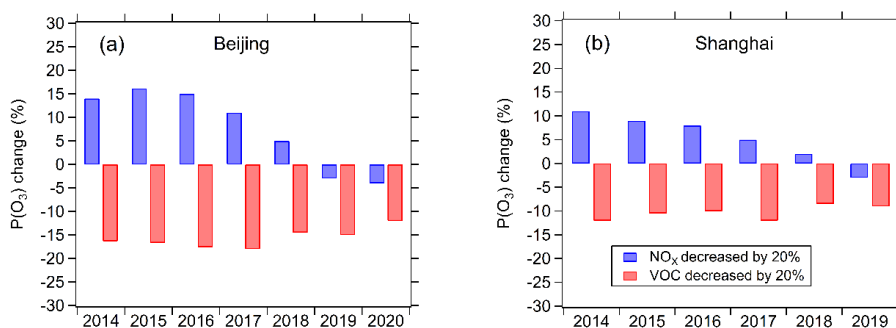


521 Figure 7. Variations in seasonal and annual average concentrations of NO<sub>2</sub> and CO  
522 measured during 2014–2020 in China.

523



524



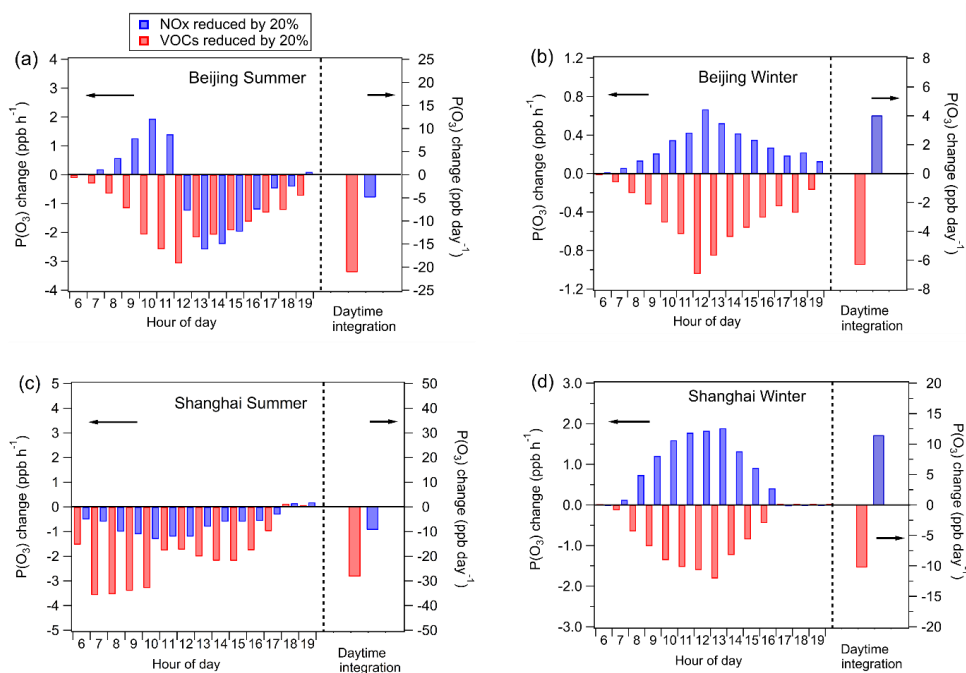
525

526 Figure 8. Sensitivity of summertime mean daytime ozone production rate [ $P(\text{O}_3)$ ] to  
527 VOCs and  $\text{NO}_x$  simulated by the photochemical box model during 2014–2020 in  
528 Beijing (a) and Shanghai (b). VOCs and  $\text{NO}_x$  are decreased by 20% to test the fractional  
529 change of  $P(\text{O}_3)$ .

530



531



532

533 Figure 9. Sensitivity of ozone production rate  $[P(\text{O}_3)]$  to 20% reductions in VOCs and  
534  $\text{NO}_x$  emissions for summer and winter 2019 in Beijing and Shanghai.

535



536

537

538 **Table 1. Description of ozone metrics used in this study.**

Metric	Definition
MDA8 (ppb)	daily maximum 8 h average, AVGMDA8 represents mean MDA8 O <sub>3</sub> in the focused period.
MDA1 (ppb)	daily maximum 1 h average; AVGMDA1 represents mean MDA1 in the focused period
4MDA8 (ppb)	The annual 4th highest MDA8 O <sub>3</sub> .
NDGT70 (days)	The annual total number of days with MDA8 O <sub>3</sub> >70 ppb.
3MMDA1	The annual maximum of the 3-month running mean of the daily maximum 1-hour ozone value. This metric has been used to quantify mortality attributable to long-term ozone exposure. The month in which the 3MMDA1 ozone concentration occurred is the middle month in the 3 months of 3MMDA1.

539

540



541

542 **Table 2. The reported trends of ozone concentration in China.**

Spatial scale	Region	Period	Metrics	Ozone trend	References
Regional scale	Eastern China	2005–2010	average ozone column	+ 0.23 DU (+1.1%) yr <sup>-1</sup>	Verstraeten et al. (2015)
	North China Plain	1979–2005	average tropospheric ozone residual	+1.1 DU (~+3%) decade <sup>-1</sup>	Xu and Lin (2011)
Urban areas	Beijing	2006–2016	MDA8	+2.6 ppb (+3.3%) yr <sup>-1</sup>	Wang et al. (2020)
	Beijing	1995–2005	daytime average	+1.0 ppb (+2.0%) yr <sup>-1</sup>	Ding et al. (2008)
	Beijing	2001–2006	daily average	+1.1 ppb (+4.1%) yr <sup>-1</sup>	Tang et al. (2009)
	Beijing	2002–2010	average ozone column	+1.6 DU (+3.1 %) yr <sup>-1</sup>	Wang et al. (2012)
	Beijing	2004–2015	MDA8	+1.14 ppb (+2.9%) yr <sup>-1</sup>	Cheng et al. (2016)
	Shanghai	2006–2016	daily average	+1.1 ppb (+6.7%) yr <sup>-1</sup>	Gao et al. (2017)
	Hong Kong	1994–2007	daytime average	+0.58 ppb (+2.0%) yr <sup>-1</sup>	Wang et al. (2009)
	Pearl River Delta	2006–2019	95 <sup>th</sup> percentile	+0.71 ppb (+1.3%) yr <sup>-1</sup>	Li et al. (2022)
	Sichuan Province	2013–2020	MDA8	+2.0 ppb (+4.8%) yr <sup>-1</sup>	Chen et al. (2021)
	Chinese urban sites	2013–2019	MDA8	+2.4 ppb (+5%) yr <sup>-1</sup>	Lu et al. (2020)
Rural sites	Shangdianzi	2004–2016	daytime average	+0.67 ppb (+1.6%) yr <sup>-1</sup>	Ma et al. (2016); Xu et al. (2020)
	Waliguan	1994–2016	daytime average	+0.21 ppb (+0.44%) yr <sup>-1</sup>	Xu et al. (2020)
	Akedala	2009–2016	daytime average	-1.3 ppb (-3.3%) yr <sup>-1</sup>	Xu et al. (2020)
	Longfengshan	2005–2016	daytime average	No trend	Xu et al. (2020)
	Lin'an	2005–2016	daytime average	No trend	Xu et al. (2020)
	Xianggelila	2007–2016	daytime average	No trend	Xu et al. (2020)
	Changdao	2013–2019	MDA8	No trend	Wang et al. (2020)

543



544 **References:**

- 545 China Statistical Yearbook in 2018, Available at <http://www.stats.gov.cn/tjsj/ndsj/2018/indexeh.htm>,  
546 45, 1817-1829, China Statistics Press, 2018.
- 547 Ainsworth, E. A., Yendrek, C. R., Sitch, S., Collins, W. J., and Emberson, L. D.: The effects of  
548 tropospheric ozone on net primary productivity and implications for climate change, *Annu.*  
549 *Rev. Plant Biol.*, 63, 637-661, 2012.
- 550 Brown-Steiner, B., and Hess, P.: Asian influence on surface ozone in the United States: A  
551 comparison of chemistry, seasonality, and transport mechanisms, *J. Geophys. Res.-Atmos.*, 116,  
552 2011.
- 553 Chen, Y., Han, H., Zhang, M., Zhao, Y., Huang, Y., Zhou, M., Wang, C., He, G., Huang, R., and Luo,  
554 B.: Trends and Variability of Ozone Pollution over the Mountain-Basin Areas in Sichuan  
555 Province during 2013–2020: Synoptic Impacts and Formation Regimes, *Atmosphere*, 12, 1557,  
556 2021.
- 557 Cheng, J., Su, J., Cui, T., Li, X., Dong, X., Sun, F., Yang, Y., Tong, D., Zheng, Y., Li, Y., Li, J., Zhang,  
558 Q., and He, K.: Dominant role of emission reduction in PM<sub>2.5</sub> air quality improvement in  
559 Beijing during 2013–2017: a model-based decomposition analysis, *Atmos. Chem. Phys.*, 19,  
560 6125-6146, 10.5194/acp-19-6125-2019, 2019.
- 561 Cheng, N., Li, Y., Zhang, D., Chen, T., Sun, F., Chen, C., and Meng, F.: Characteristics of ground  
562 ozone concentration over Beijing from 2004 to 2015: Trends, transport, and effects of  
563 reductions, *Atmos. Chem. Phys.*, 2016.
- 564 Cooper, O. R., Parrish, D., Stohl, A., Trainer, M., Nédélec, P., Thouret, V., Cammas, J.-P., Oltmans,  
565 S., Johnson, B., and Tarasick, D.: Increasing springtime ozone mixing ratios in the free  
566 troposphere over western North America, *Nature*, 463, 344-348, 2010.
- 567 Cooper, O. R., Gao, R. S., Tarasick, D., Leblanc, T., and Sweeney, C.: Long-term ozone trends at  
568 rural ozone monitoring sites across the United States, 1990–2010, *J. Geophys. Res.-Atmos.*,  
569 117, 2012.
- 570 Ding, A., Wang, T., Thouret, V., Cammas, J.-P., and Nédélec, P.: Tropospheric ozone climatology  
571 over Beijing: analysis of aircraft data from the MOZAIC program, *Atmos. Chem. Phys.*, 8, 1-  
572 13, 2008.
- 573 Fiore, A. M., Dentener, F., Wild, O., Cuvelier, C., Schultz, M., Hess, P., Textor, C., Schulz, M.,  
574 Doherty, R., and Horowitz, L.: Multimodel estimates of intercontinental source-receptor  
575 relationships for ozone pollution, *J. Geophys. Res.-Atmos.*, 114, 2009.
- 576 Fleming, Z. L., Doherty, R. M., Von Schneidmesser, E., Malley, C. S., Cooper, O. R., Pinto, J. P.,  
577 Colette, A., Xu, X., Simpson, D., and Schultz, M. G.: Tropospheric Ozone Assessment Report:  
578 Present-day ozone distribution and trends relevant to human health, *Elem. Sci. Anth.*, 6, 12,  
579 2018.
- 580 Gao, W., Tie, X. X., Xu, J. M., Huang, R. J., Mao, X. Q., Zhou, G. Q., and Chang, L. Y.: Long-term  
581 trend of O<sub>3</sub> in a mega City (Shanghai), China: Characteristics, causes, and interactions with  
582 precursors, *Sci. Total Environ.*, 603, 425-433, 10.1016/j.scitotenv.2017.06.099, 2017.
- 583 Hendrick, F., Müller, J.-F., Clémer, K., Wang, P., De Mazière, M., Fayt, C., Gielen, C., Hermans, C.,  
584 Ma, J., and Pinardi, G.: Four years of ground-based MAX-DOAS observations of HONO and  
585 NO<sub>2</sub> in the Beijing area, *Atmos. Chem. Phys.*, 14, 765-781, 2014.
- 586 Jiang, H., Lu, N., Qin, J., and Yao, L.: Surface global and diffuse solar radiation over China acquired



- 587 from geostationary Multi-functional Transport Satellite data, *Earth System Science Data*  
588 *Discussions*, 1-22, 2019.
- 589 Jindal, S.: Air quality guidelines: Global update 2005, Particulate matter, ozone, nitrogen dioxide  
590 and sulfur dioxide, *Indian J. Med. Res.*, 126, 492-494, 2007.
- 591 Kang, M., Zhang, J., Zhang, H., and Ying, Q.: On the Relevancy of Observed Ozone Increase during  
592 COVID-19 Lockdown to Summertime Ozone and PM<sub>2.5</sub> Control Policies in China, *Environ.*  
593 *Sci. Technol. Lett.*, 8, 289-294, 2021.
- 594 Kleinman, L. I.: Low and high NO<sub>x</sub> tropospheric photochemistry, *J. Geophys. Res.-Atmos.*, 99,  
595 16831-16838, 1994.
- 596 Kleinman, L. I., Daum, P. H., Lee, J. H., Lee, Y. N., Nunnermacker, L. J., Springston, S. R., Newman,  
597 L., Weinstein-Lloyd, J., and Sillman, S.: Dependence of ozone production on NO and  
598 hydrocarbons in the troposphere, *Geophys. Res. Lett.*, 24, 2299-2302, 1997.
- 599 Le, T., Wang, Y., Liu, L., Yang, J., Yung, Y. L., Li, G., and Seinfeld, J. H.: Unexpected air pollution  
600 with marked emission reductions during the COVID-19 outbreak in China, *Science*, 369, 702-  
601 706, 2020.
- 602 Li, J., Lu, K., Lv, W., Li, J., Zhong, L., Ou, Y., Chen, D., Huang, X., and Zhang, Y.: Fast increasing  
603 of surface ozone concentrations in Pearl River Delta characterized by a regional air quality  
604 monitoring network during 2006–2011, *J. Environ. Sci.*, 26, 23-36, 2014.
- 605 Li, K., Jacob, D. J., Liao, H., Shen, L., Zhang, Q., and Bates, K. H.: Anthropogenic drivers of 2013–  
606 2017 trends in summer surface ozone in China, *Proc. National Acad. Sci.*, 116, 422-427, 2019a.
- 607 Li, K., Jacob, D. J., Shen, L., Lu, X., De Smedt, I., and Liao, H.: Increases in surface ozone pollution  
608 in China from 2013 to 2019: anthropogenic and meteorological influences, *Atmos. Chem.*  
609 *Phys.*, 20, 11423-11433, 2020.
- 610 Li, K., Jacob, D. J., Liao, H., Qiu, Y., Shen, L., Zhai, S., Bates, K. H., Sulprizio, M. P., Song, S., and  
611 Lu, X.: Ozone pollution in the North China Plain spreading into the late-winter haze season,  
612 *Proc. National Acad. Sci.*, 118, 2021.
- 613 Li, M., Zhang, Q., Zheng, B., Tong, D., Lei, Y., Liu, F., Hong, C., Kang, S., Yan, L., and Zhang, Y.:  
614 Persistent growth of anthropogenic non-methane volatile organic compound (NMVOC)  
615 emissions in China during 1990–2017: drivers, speciation and ozone formation potential,  
616 *Atmos. Chem. Phys.*, 19, 8897-8913, 2019b.
- 617 Li, X.-B., Yuan, B., Parrish, D. D., Chen, D., Song, Y., Yang, S., Liu, Z., and Shao, M.: Long-term  
618 trend of ozone in southern China reveals future mitigation strategy for air pollution, *Atmos.*  
619 *Environ.*, 269, 118869, 2022.
- 620 Lin, M., Fiore, A. M., Horowitz, L. W., Cooper, O. R., Naik, V., Holloway, J., Johnson, B. J.,  
621 Middlebrook, A. M., Oltmans, S. J., and Pollack, I. B.: Transport of Asian ozone pollution into  
622 surface air over the western United States in spring, *J. Geophys. Res.-Atmos.*, 117, 2012.
- 623 Liu, F., Zhang, Q., Zheng, B., Tong, D., Yan, L., Zheng, Y., and He, K.: Recent reduction in NO<sub>x</sub>  
624 emissions over China: synthesis of satellite observations and emission inventories, *Environ.*  
625 *Res. Lett.*, 11, 114002, 2016.
- 626 Liu, H., Liu, S., Xue, B., Lv, Z., Meng, Z., Yang, X., Xue, T., Yu, Q., and He, K.: Ground-level  
627 ozone pollution and its health impacts in China, *Atmos. Environ.*, 173, 223-230, 2018.
- 628 Lu, X., Hong, J. Y., Zhang, L., Cooper, O. R., Schultz, M. G., Xu, X. B., Wang, T., Gao, M., Zhao,  
629 Y. H., and Zhang, Y. H.: Severe Surface Ozone Pollution in China: A Global Perspective,  
630 *Environ. Sci. Technol. Lett.*, 5, 487-494, 10.1021/acs.estlett.8b00366, 2018.



- 631 Lu, X., Zhang, L., Wang, X., Gao, M., Li, K., Zhang, Y., Yue, X., and Zhang, Y.: Rapid increases in  
632 warm-season surface ozone and resulting health impact in China since 2013, *Environ. Sci.*  
633 *Technol. Lett.*, 7, 240-247, 2020.
- 634 Ma, Z. Q., Xu, J., Quan, W. J., Zhang, Z. Y., Lin, W. L., and Xu, X. B.: Significant increase of  
635 surface ozone at a rural site, north of eastern China, *Atmos. Chem. Phys.*, 16, 3969-3977,  
636 10.5194/acp-16-3969-2016, 2016.
- 637 Malley, C. S., Henze, D. K., Kuylenstierna, J. C., Vallack, H. W., Davila, Y., Anenberg, S. C., Turner,  
638 M. C., and Ashmore, M. R.: Updated global estimates of respiratory mortality in adults  $\geq 30$   
639 years of age attributable to long-term ozone exposure, *Environ. Health Perspect.*, 125, 087021,  
640 2017.
- 641 Mihelcic, D., Holland, F., Hofzumahaus, A., Hoppe, L., Konrad, S., M $\ddot{u}$ sgen, P., P $\ddot{a}$ tz, H. W., Sch $\ddot{a}$ fer,  
642 H. J., Schmitz, T., and Volz-Thomas, A.: Peroxy radicals during BERLIOZ at Pabstthum:  
643 Measurements, radical budgets and ozone production, *J. Geophys. Res.-Atmos.*, 108, 2003.
- 644 Mills, G., Pleijel, H., Malley, C. S., Sinha, B., Cooper, O. R., Schultz, M. G., Neufeld, H. S.,  
645 Simpson, D., Sharps, K., and Feng, Z.: Tropospheric Ozone Assessment Report: Present-day  
646 tropospheric ozone distribution and trends relevant to vegetation, *Elem. Sci. Anth.*, 6, 2018.
- 647 Monks, P. S., Archibald, A., Colette, A., Cooper, O., Coyle, M., Derwent, R., Fowler, D., Granier,  
648 C., Law, K. S., and Mills, G.: Tropospheric ozone and its precursors from the urban to the  
649 global scale from air quality to short-lived climate forcer, *Atmos. Chem. Phys.*, 15, 8889-8973,  
650 2015.
- 651 Parrish, D. D., Derwent, R. G., Steinbrecht, W., St $\ddot{u}$ bi, R., Van Malderen, R., Steinbacher, M., Trickl,  
652 T., Ries, L., and Xu, X.: Zonal similarity of long-term changes and seasonal cycles of baseline  
653 ozone at northern midlatitudes, *J. Geophys. Res.-Atmos.*, 125, e2019JD031908, 2020.
- 654 Qu, K., Wang, X., Yan, Y., Shen, J., Xiao, T., Dong, H., Zeng, L., and Zhang, Y.: A comparative  
655 study to reveal the influence of typhoons on the transport, production and accumulation of O $_3$   
656 in the Pearl River Delta, China, *Atmos. Chem. Phys.*, 21, 11593-11612, 2021.
- 657 Shah, V., Jacob, D. J., Li, K., Silvern, R. F., Zhai, S. X., Liu, M. Y., Lin, J. T., and Zhang, Q.: Effect  
658 of changing NO $_x$  lifetime on the seasonality and long-term trends of satellite-observed  
659 tropospheric NO $_2$  columns over China, *Atmos. Chem. Phys.*, 20, 1483-1495, 10.5194/acp-20-  
660 1483-2020, 2020.
- 661 Shao, M., Wang, W., Yuan, B., Parrish, D. D., Li, X., Lu, K., Wu, L., Wang, X., Mo, Z., and Yang,  
662 S.: Quantifying the role of PM $_2.5$  dropping in variations of ground-level ozone: Inter-  
663 comparison between Beijing and Los Angeles, *Sci. Total Environ.*, 147712, 2021.
- 664 Stevenson, D., Dentener, F., Schultz, M., Ellingsen, K., Van Noije, T., Wild, O., Zeng, G., Amann,  
665 M., Atherton, C., and Bell, N.: Multimodel ensemble simulations of present-day and near-  
666 future tropospheric ozone, *J. Geophys. Res.-Atmos.*, 111, 2006.
- 667 Stocker, T. F., Qin, D., Plattner, G.-K., Tignor, M. M., Allen, S. K., Boschung, J., Nauels, A., Xia,  
668 Y., Bex, V., and Midgley, P. M.: Climate Change 2013: The physical science basis. contribution  
669 of working group I to the fifth assessment report of IPCC the intergovernmental panel on  
670 climate change, 2014.
- 671 Stohl, A., Bonasoni, P., Cristofanelli, P., Collins, W., Feichter, J., Frank, A., Forster, C.,  
672 Gerasopoulos, E., G $\ddot{a}$ ggeler, H., and James, P.: Stratosphere-troposphere exchange: A review,  
673 and what we have learned from STACCATO, *J. Geophys. Res.-Atmos.*, 108, 2003.
- 674 Sun, L., Xue, L., Wang, T., Gao, J., Ding, A., Cooper, O. R., Lin, M., Xu, P., Wang, Z., and Wang,



- 675 X.: Significant increase of summertime ozone at Mount Tai in Central Eastern China, *Atmos.*  
676 *Chem. Phys.*, 16, 10637-10650, 2016.
- 677 Tang, G., Li, X., Wang, Y., Xin, J., and Ren, X.: Surface ozone trend details and interpretations in  
678 Beijing, 2001–2006, *Atmos. Chem. Phys.*, 9, 8813-8823, 2009.
- 679 Tang, G., Liu, Y., Zhang, J., Liu, B., Li, Q., Sun, J., Wang, Y., Xuan, Y., Li, Y., and Pan, J.: Bypassing  
680 the NO<sub>x</sub> titration trap in ozone pollution control in Beijing, *Atmos. Res.*, 249, 105333, 2021.
- 681 Trickl, T., Bärtsch-Ritter, N., Eisele, H., Furger, M., Mücke, R., Sprenger, M., and Stohl, A.: High-  
682 ozone layers in the middle and upper troposphere above Central Europe: potential import from  
683 the stratosphere along the subtropical jet stream, *Atmos. Chem. Phys.*, 11, 9343-9366, 2011.
- 684 Verstraeten, W. W., Neu, J. L., Williams, J. E., Bowman, K. W., Worden, J. R., and Boersma, K. F.:  
685 Rapid increases in tropospheric ozone production and export from China, *Nat. Geosci.*, 8, 690-  
686 +, 10.1038/ngeo2493, 2015.
- 687 Wang, B., Shao, M., Lu, S. H., Yuan, B., Zhao, Y., Wang, M., Zhang, S. Q., and Wu, D.: Variation  
688 of ambient non-methane hydrocarbons in Beijing city in summer 2008, *Atmos. Chem. Phys.*,  
689 10, 5911-5923, 10.5194/acp-10-5911-2010, 2010.
- 690 Wang, T., Wei, X., Ding, A., Poon, C., Lam, K. S., Li, Y. S., Chan, L., and Anson, M.: Increasing  
691 surface ozone concentrations in the background atmosphere of Southern China, 1994–2007,  
692 *Atmos. Chem. Phys.*, 9, 6217-6227, 2009.
- 693 Wang, W., Li, X., Shao, M., Hu, M., Zeng, L., Wu, Y., and Tan, T.: The impact of aerosols on  
694 photolysis frequencies and ozone production in Beijing during the 4-year period 2012–2015,  
695 *Atmos. Chem. Phys.*, 19, 9413-9429, 10.5194/acp-19-9413-2019, 2019.
- 696 Wang, W., Parrish, D. D., Li, X., Shao, M., Liu, Y., Mo, Z., Lu, S., Hu, M., Fang, X., and Wu, Y.:  
697 Exploring the drivers of the increased ozone production in Beijing in summertime during  
698 2005–2016, *Atmos. Chem. Phys.*, 20, 15617-15633, 2020.
- 699 Wang, W., van der A, R., Ding, J., van Weele, M., and Cheng, T.: Spatial and temporal changes of  
700 the ozone sensitivity in China based on satellite and ground-based observations, *Atmos. Chem.*  
701 *Phys.*, 21, 7253-7269, 10.5194/acp-21-7253-2021, 2021.
- 702 Wang, Y., Konopka, P., Liu, Y., Chen, H., Müller, R., Plöger, F., Riese, M., Cai, Z., and Lü, D.:  
703 Tropospheric ozone trend over Beijing from 2002–2010: ozonesonde measurements and  
704 modeling analysis, *Atmos. Chem. Phys.*, 12, 8389-8399, 2012.
- 705 Xiao, Z., and Jiang, H.: A study of spatial and temporal dynamics of total ozone over Southwest  
706 China with multi-source remote-sensing data, *Int. J. Remote Sens.*, 34, 128-138, 2013.
- 707 Xu, J., Ma, J. Z., Zhang, X. L., Xu, X. B., Xu, X. F., Lin, W. L., Wang, Y., Meng, W., and Ma, Z. Q.:  
708 Measurements of ozone and its precursors in Beijing during summertime: impact of urban  
709 plumes on ozone pollution in downwind rural areas, *Atmos. Chem. Phys.*, 11, 12241-12252,  
710 10.5194/acp-11-12241-2011, 2011.
- 711 Xu, J., Tie, X., Gao, W., Lin, Y., and Fu, Q.: Measurement and model analyses of the ozone variation  
712 during 2006 to 2015 and its response to emission change in megacity Shanghai, China, *Atmos.*  
713 *Chem. Phys.*, 19, 9017-9035, 10.5194/acp-19-9017-2019, 2019.
- 714 Xu, W., Lin, W., Xu, X., Tang, J., Huang, J., Wu, H., and Zhang, X.: Long-term trends of surface  
715 ozone and its influencing factors at the Mt Waliguan GAW station, China – Part I: Overall  
716 trends and characteristics, *Atmos. Chem. Phys.*, 16, 6191-6205, 10.5194/acp-16-6191-2016,  
717 2016.
- 718 Xu, W., Xu, X., Lin, M., Lin, W., Tarasick, D., Tang, J., Ma, J., and Zheng, X.: Long-term trends of



719 surface ozone and its influencing factors at the Mt Waliguan GAW station, China – Part 2: The  
720 roles of anthropogenic emissions and climate variability, *Atmos. Chem. Phys.*, 18, 773-798,  
721 10.5194/acp-18-773-2018, 2018.

722 Xu, X., Lin, W., Wang, T., Yan, P., Tang, J., Meng, Z., and Wang, Y.: Long-term trend of surface  
723 ozone at a regional background station in eastern China 1991–2006: enhanced variability,  
724 *Atmos. Chem. Phys.*, 8, 2595-2607, 2008.

725 Xu, X., and Lin, W.: Trends of tropospheric ozone over China based on satellite data (1979–2005),  
726 *Adv. Clim. Chang. Res.*, 2, 43-48, 2011.

727 Xu, X., Lin, W., Xu, W., Jin, J., Wang, Y., Zhang, G., Zhang, X., Ma, Z., Dong, Y., and Ma, Q.:  
728 Long-term changes of regional ozone in China: implications for human health and ecosystem  
729 impacts, *Elem. Sci. Anth.*, 8, 2020.

730 Yin, C., Solmon, F., Deng, X., Zou, Y., Deng, T., Wang, N., Li, F., Mai, B., and Liu, L.: Geographical  
731 distribution of ozone seasonality over China, *Sci. Total Environ.*, 689, 625-633, 2019.

732 Young, P., Archibald, A., Bowman, K., Lamarque, J.-F., Naik, V., Stevenson, D., Tilmes, S.,  
733 Voulgarakis, A., Wild, O., and Bergmann, D.: Pre-industrial to end 21st century projections of  
734 tropospheric ozone from the Atmospheric Chemistry and Climate Model Intercomparison  
735 Project (ACCMIP), *Atmos. Chem. Phys.*, 13, 2063-2090, 2013.

736 Zhang, J. P., Zhu, T., Zhang, Q. H., Li, C. C., Shu, H. L., Ying, Y., Dai, Z. P., Wang, X., Liu, X. Y.,  
737 Liang, A. M., Shen, H. X., and Yi, B. Q.: The impact of circulation patterns on regional  
738 transport pathways and air quality over Beijing and its surroundings, *Atmos. Chem. Phys.*, 12,  
739 5031-5053, 10.5194/acp-12-5031-2012, 2012.

740 Zhang, Q., Yuan, B., Shao, M., Wang, X., Lu, S., Lu, K., Wang, M., Chen, L., Chang, C.-C., and  
741 Liu, S.: Variations of ground-level O<sub>3</sub> and its precursors in Beijing in summertime between  
742 2005 and 2011, *Atmos. Chem. Phys.*, 14, 6089-6101, 2014.

743 Zheng, B., Zhang, Q., Geng, G., Chen, C., Shi, Q., Cui, M., Lei, Y., and He, K.: Changes in China's  
744 anthropogenic emissions and air quality during the COVID-19 pandemic in 2020, *Earth Syst.*  
745 *Sci. Data*, 13, 2895-2907, 10.5194/essd-13-2895-2021, 2021.

746

747

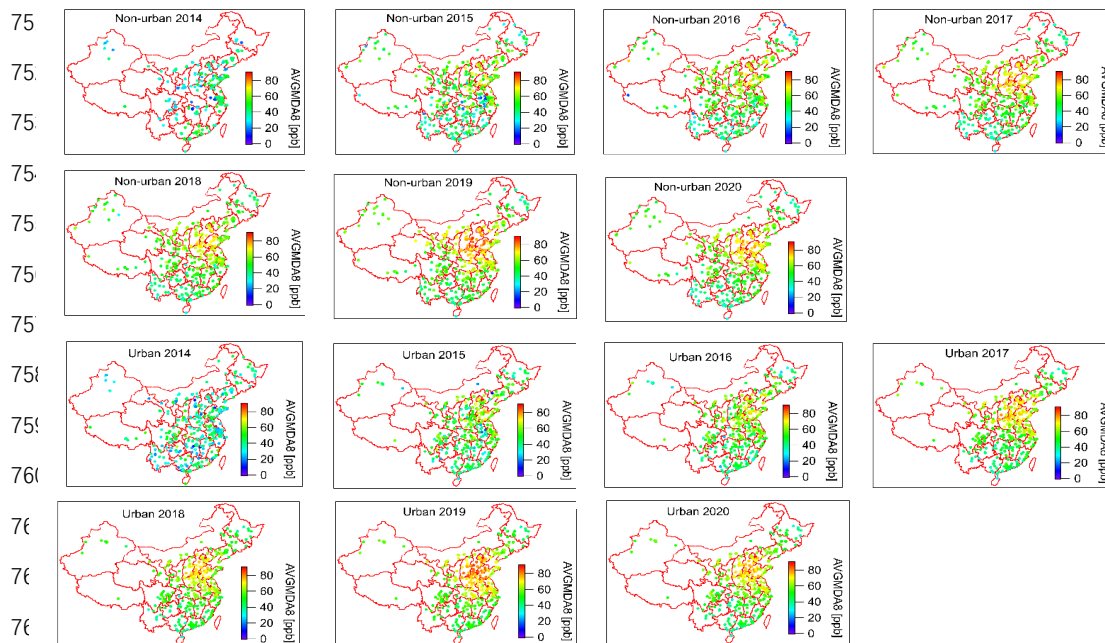


748

749

## Appendix

750



764

765 Figure A1. Spatial distribution of warm-season AVGMDA8 ozone concentrations in  
766 urban and non-urban areas during 2014-2020.

767

768

769

770

771

772

773

774

775

776